# Dynamics of shock waves excited by a high-current relativistic electron beam in aluminum targets

A. F. Akkerman, A. V. Bushman, B. A. Demidov, M. V. Ivkin, A. L. Ni, V. A. Petrov, L. I. Rudakov, and V. E. Fortov

(Submitted 18 March 1985)

Experiments are described on the generation of shock waves in the megabar pressure range excited by a high-current relativistic electron beam in aluminum targets. The data are compared with the results found by one- and two-dimensional numerical simulation.

## 1. INTRODUCTION

The idea of achieving controlled fusion with inertial plasma confinement is based on using pulsed energy beams (lasers, electron or ion beams, fast shock waves) to heat the reactants and compress them by a factor of $10^3-10^4$ (Refs. 1,2). In order to analyze the physical processes and optimize the microtargets and irradiation conditions, one must know the physical properties of the fuel in a large region of the phase diagram extending from STP up to extremely high pressures $10^8-10^9$ bar (Ref. 3), and the time-dependent motion of dense plasmas heated rapidly by intense pulses must also be understood.

Most of our current knowledge regarding the thermophysical properties of materials at megabar pressures comes from dynamic experiments in which chemical and high explosives are detonated to set off powerful shock waves that compress and irreversibly heat the material.[4,5] More powerful excitation sources, such as laser, electroexplosive, and electrodynamic devices,[6] have also recently been considered in order to increase the peak pressures further. High-current relativistic electron beams (REB) have some important advantages in high pressure generation—the evolved power is greater than can be achieved by chemical explosives, while the volume of the shock-compressed plasma is substantially greater than in laser devices.

Early experimental work revealed that when a focused high-current REB strikes a metal target, shock waves are generated with peak pressures of several Mbar even for moderate REB power densities $\approx 10^{16}$ W/m$^2$ (Refs. 7,8). Power densities of $5 \cdot 10^{17}$ W/m$^2$ have already been achieved with sharply focused beams,[9] and estimates show that these powers should suffice to generate pressures in excess of 10 Mbar (Ref. 10). In view of the continual technical advances in intense REB generation one may thus hope to reach dynamic pressures in the tens-of-megabar range.

The purpose of the present paper is to analyze how intense shock waves are generated in metals and assess diagnostic techniques for studying the motion of shock-compressed plasmas so that high–current REBs can be used to analyze the equation of state of materials at megabar pressures.

## 2. EXPERIMENTAL METHOD AND RESULTS

As usual in dynamic methods,[4–6] the determination of the equation of state of a shock-compressed material reduces to independently measuring the kinematic propagation parameters of plane steady shock waves and then invoking mass, momentum, and energy conservation to deduce the thermodynamic properties. Our interest in this paper is therefore focused on measuring the front and flow velocities $D$ and $U$ of the shock waves. The intense electromagnetic noise from the REB generator makes it difficult to employ electrical-contact and manganin techniques in dynamic measurements, so that optical methods using flexible quartz light quides are necessary.[11]

The experiments were carried out on the "Kal'mar" high-current electron accelerator[12] with beam current 80 kA, electron energy 0.35 MeV, current pulse length 100 ns (half-maximum), focal spot diameter 2 mm, and total REB energy $\approx 1$ kJ in the focal spot. We used the stepped target method[4,5] to measure the shock wave velocity $D$ and the mass velocity $U$. Figure 1 shows the experimental system. The cathode 1 housed in the vacuum diode chamber 2 of the accelerator emits an electron beam 3, which strikes an aluminum plate (anode) 4 and excites a shock wave in it. The back side of the anode plate borders an air gap 5, which is bounded on the other side by a 2-mm-thick plastic plate 7. A flexible quartz light guide 8 is located 4 mm from the plastic plate directly opposite the center of the anode plate; the light guide is 15 m long and 0.8 mm in diameter (including the polyethylene sheath).[11] A similar light guide 10 is optically connected to an x-ray detector 11 (stilbene crystal) mounted in a centering sleeve 9. The opposite ends of the light guides are enclosed in a shielded diagnostic chamber and located next to an FÉU- 30 photomultiplier with time reso-
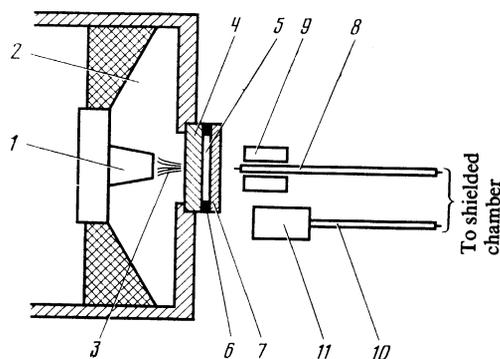


FIG. 1. Sketch of experimental system: 1) cathode; 2) vacuum diode chamber of accelerator; 3) REB; 4) anode plate (target); 5) air gap; 6) spacer; 7) plastic plate; 8) light guide; 9) centering sleeve; 10) light-emitting diode; 11) x-ray detector.
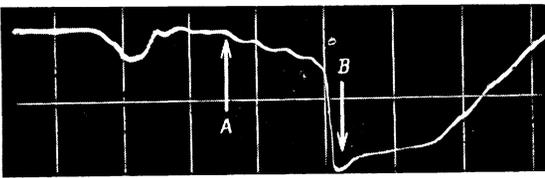
FIG. 2. Trace of a shock wave propagating in an aluminum plate of thickness 1.5 mm (the air gap was 0.6 mm wide).

lution better than 2–3 ns. The output signal from the FÉU-30 is input to an S1-11 oscilloscope through a 75-ohm resistor.

Figure 2 shows a trace of a shock wave propagating in a 1.5-mm-thick aluminum plate. The first dip is due to the signal from the x-ray detector, which records the Bremsstrahlung burst at the instant the REB hits the target and serves as a precise time reference. When the shock wave reaches the back side of the plate, the latter starts to move at nearly twice the mass velocity and a shock wave is generated in the air gap, causing the air to glow. This shows up in the trace as a weak dip (indicated by the arrow $A$). This dip (which corresponds to an increase in the signal amplitude) is caused by the growth of a layer of shock-compressed air plasma between the shock discontinuity and the moving aluminum plate. This causes the emission intensity to increase with time at nearly the same rate as was found experimentally in Ref. 13, where the rise in the intensity was used to deduce the absorption coefficient of the shock-compressed plasma. The signal amplitude gradually increases and peaks when the contact surface and plastic plate are in immediate contact. At this instant (indicated by arrow $B$ in Fig. 2) the plastic shatters and the signal amplitude starts to drop because the plastic becomes less transparent. The trace can thus be used to deduce the time required for the shock wave to reach the back side of the aluminum plate and to determine the instant when the contact surface strikes the plastic plate. The time during which the contact surface moves can then be found, from which the mass velocity $U$ of the shock wave follows since the width of the air gap is known.

The curves in Fig. 3 indicate the times when the shock wave reaches the back side of aluminum plates of various thicknesses $x$ (curve 1) and the times when the contact surface strikes the plastic plate; curves 2 and 3 are for air gaps

0.1 mm and 0.6 mm wide, respectively. The curves lie farther apart along the $\tau$ axis as $x$ increases, which indicates that the shock waves are damped for large $x$ because of decompression waves on the edges and back side of the plate (this is confirmed by direct hydrodynamic calculations). Curve 1 in Fig. 3 can be used to find the velocity $D$ of the shock wave, while curves 2 and 3 give the characteristic velocity $W$ of the back side of the target, which expands adiabatically. This method for determining the kinematic parameters of the shock wave overestimates $D$ by 15–20% because it neglects the region of the target in which the bulk energy evolution generates the shock wave. We eliminated this error by employing a target plate with a step profile.[14,15] This enabled us to carry out the measurements on the base of the step, away from the hot spot and within the region where the shock wave was generated and the heating of the target by the electrons was minimal. This was done by mounting the two light guides at the center of the back side of the aluminum plate; they were separated by a distance of 2.5 mm in order to eliminate mutual interference. One of the light guides was imbedded in the target to a depth of 0.2–1.0 mm (this established a measurement scale). The opposite ends of the light guides were located near the photocathode of the FÉU-30.

Figure 4 shows a trace of a shock wave propagating in a 2-mm-thick aluminum plate with a 1 mm step. The first dip in the trace serves as a reference for the instant the electron beam strikes the aluminum plate. The arrow $A$ marks the second negative signal, which has a steep edge and occurs when the shock wave reaches the first light guide. We see that this occurs when the electron beam has essentially stopped interacting with the target and the shock wave has already formed. The third negative signal (arrow $B$) also drops abruptly; it indicates the time when the shock wave reaches the back side of the aluminum plate. For a given step height, the shock wave velocity $D$ can be found by measuring the time interval between the edges of the second and third pulses. Figure 5 shows the results of these measurements.

As a further check on our measurements of the mass velocity $U$, we measured the transit time $W$ for the shattered aluminum fragments to cross a vacuum gap. We used the time-of-flight method with a 34-cm-long baseline. The recording device, an electrocontact detector, was triggered when an aluminum fragment pierced an aluminum or lavsan plastic foil of thickness 35 and 25 $\mu$m, respectively.

Figure 5 shows the experimental results found by various methods for the damping of the shock wave velocity $D$ and mass velocity $U$ with penetration into the target. We used the doubling rule[4,5] $W = 2U$ to relate $U$ to the velocity $W$ of the back side of the target plate; this is reasonable be-
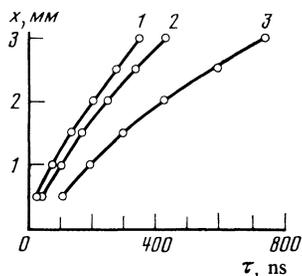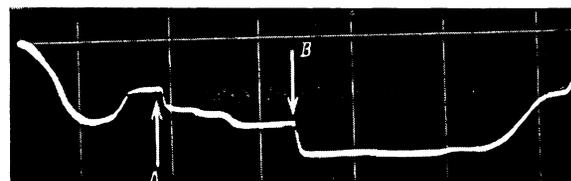


FIG. 3. Time required for the shock wave to reach the back side of the target (curve 1) and for the contact surface to strike the plastic plate for air gaps 0.1 and 0.6 mm wide (curves 2 and 3, respectively) and several target thicknesses.



FIG. 4. Trace of a shock wave propagating in a 2-mm-thick aluminum plate (1 mm scale of measurement).
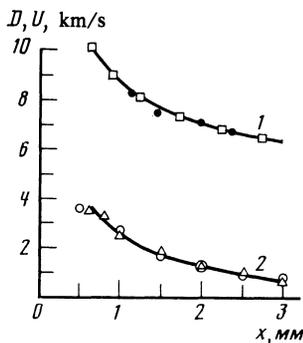
$D, U$, km/s



FIG. 5. Propagation and mass velocities $D$ (1) and $U$ (2) of a shock wave as a function of the distance $x$ measured from the front plane of the aluminum anode plate: O, time-of-flight measurements; □, measurements from optical scanning of the targets (with air gap and plastic plate); △, two-step method using light guides; ●, data found by analyzing all the points on curve 1, Fig. 3.

cause according to the entropy condition stated in Refs. 4 and 16, the shock wave amplitudes $P \leqslant 1$ Mbar under our conditions were too low for the aluminum to vaporize in the decompression wave.

Figure 5 shows that the various methods for measuring the shock wave velocities in REB experiments yield similar results. These techniques can therefore be used to determine the equation of state of shock-compressed metals by the reflection method[4,5] by recording the shock wave velocities for waves impinging on the sample from a standard reference material. The experiments indicate that the shock waves are appreciably damped, so that the dynamics of shock wave generation and decay in REB experiments requires more detailed analysis.

## 3. NUMERICAL SIMULATION OF SHOCK WAVE GENERATION AND DAMPING

We were primarily interested in simulating the shock-wave processes inside the condensed target and only secondarily in the properties of the expanding plasma. The latter were analyzed in Ref. 17 with allowance for corona emission for REBs interacting with metal targets.

We consider the following qualitative model for REB-target interaction. The electrons moving in the target lose energy in inelastic collisions with the target electrons and through Bremsstrahlung. Elastic collisions with atomic nuclei cause the trajectories to veer off in random directions, so that the electrons can be regarded as diffusing into the target. If the target is heated by a laser, light energy is absorbed in a low-density plasma that expands into the beam; this energy then acts as a thermal wave and heats up a target layer of thickness $\sim 1 \mu m$ (Ref. 18). By contrast, an electron beam penetrates much deeper into the target (to 200–300 $\mu m$ in our experiments) and bulk-heating occurs. During the beam pulse the volume of the hot zone increases only severalfold, while its temperature reaches 20–30 eV. Under these conditions we can use the one-fluid approximation and neglect radiative and electronic heat conduction.

Heating of thin (3–10 $\mu m$) heavy-metal foils by sharply focused high-current beams was studied experimentally in Ref. 19 (some of the beams were generated by the Kal'mar

accelerator). The energy deposited in the foil was found to be greater than for low-current beams for which $I < 17,000$ $\beta \gamma$ [kA] holds, where $\beta = v/c$ and $\gamma = 1/(1 - \beta^2)^{1/2}$ are the usual relativistic factors. The deposited energy increased because the magnetization of the beam electrons[20] in the sputtered foil plasma lengthened the trajectories by a factor of $\sim I/17,000 \beta \gamma$. Because of the high density of the aluminum plasma, the magnetization in these experiments was weak: $\omega_H \tau_{ei} \approx 1$, even though the penetration distance $\delta \sim (c^2 t/4\pi\sigma)^{1/2} \sim 10^{-1}$ cm of the magnetic field into the plasma was comparable to the width of the hot sputtered layer (here $\omega_H$ is the electron cyclotron frequency, $\tau_{ei}$ is the electron-ion interaction time, and the plasma conductivity $\sigma$ is taken to be $\approx 10^{15}$ s$^{-1}$). However, we will neglect the increased energy evolution in our calculation. The time-dependent gasdynamic equations

$$\frac{\partial \rho}{\partial t} + \mathrm{div}\, \rho\, \mathbf{U} = 0,$$

$$\frac{\partial \rho \mathbf{U}}{\partial t} + \mathrm{div}\, \rho \mathbf{U}\mathbf{U} - \mathrm{grad}\, P = 0,$$

$$\frac{\partial \rho e \mathbf{U}}{\partial t} + \mathrm{div}\, \rho e \mathbf{U} + \mathrm{div}\, P\mathbf{U} = q$$

govern the motion of a compressible continuous medium and correspond to mass, momentum, and energy conservation, respectively. Here $U$ is the velocity vector, $P$ is the pressure, $\rho$ is the density, $e = U^2/2 + E(P,V)$ is the total specific energy, $E(P,V)$ is the specific internal energy, and the source term $q$ describes the volume deposition of the REB energy.

The physical properties of aluminum were described by the semiempirical equation of state[21] $P = P(E,V)$ deduced from available experimental and theoretical data. This equation is consistent with data on the thermodynamic properties of the solid, liquid, gaseous, and plasma phases; moreover, it allows for ionization, includes heat-of-fusion and vaporization effects, and agrees with the Thomas-Fermi and Debye-Hückel theories in the limit $P,T \to \infty$ (Ref. 3). We used the equation of state in tabulated form in the gasdynamic calculations.

The equations of motion were solved by the Godunov numerical scheme,[22] which is accurate to first order on regular grids and possesses the property of monotonicity. The surface of the target and the axis of symmetry bounded the computational region. Two of these boundaries—the lines bounding the corona and the back side of the target—moved spatially as required by the condition that the pressure on them be constant. Since the target radius was assumed large enough so that the pressure waves did not reach the edges of the plate for the times considered, the edges did not move. The number of gridpoints varied and increased with the size of the regions bounded by the corona line and back side of the target.

We used the Monte-Carlo method with allowance for elastic electron-nucleus, electron-electron, and inelastic stopping collisions[23] to calculate the energy deposited in the target by the REB for a specified density profile calculated from the hydrodynamic equations. In the Monte-Carlo

method each electron trajectory (representing the "history" of the electron) is a broken line; the electron is elastically scattered at the vertices and changes direction, but between collisions it follows a straight line and its kinetic energy decreases due to ionization and Bremsstrahlung losses. Each trajectory was thus stored in the computer as a sequence of 4-tuples $\{x_n, y_n, z_n, E_n^*\}$, where $x_n, y_n, z_n$ are the coordinates of the $n$th vertex and $E_n^*$ is the energy transferred by the electron to the target between vertices $n$ and $n + 1$. We rescaled the electron energy losses for materials with a spatially varying density $\rho(x, y, z)$ by assuming that the scattering angles in each elastic collision event were the same as in a homogeneous target. The length of each interval between two vertices was scaled by the factor $\rho_0/\rho(x, y, z)$, where $\rho_0$ is the "normal" density for which the energy deposition was previously calculated. The energy loss per unit length at the point $(x, y, z)$ was then given by

$$dE^* = \frac{E_n^* \rho(x, y, z)}{\Delta l_n \rho_0},$$

$$\Delta l_n = [(x_{n+1} - x_n)^2 + (y_{n+1} - y_n)^2 + (z_{n+1} - z_n)^2]^{1/2},$$

where $\Delta l_n$ is the length of the segment joining vertices $n$ and $n + 1$. The energy deposited by the REB was then found by averaging over a number $N \sim 10,000$ of trajectories, which was chosen so that the error due to random fluctuations was comparable to the error in the numerical method used to solve the gasdynamic equation.

The beam parameters were chosen to correspond to the experimental conditions: beam density

$$j = \begin{cases} j_0 \sin(\pi\tau/T), & 0 < \tau < T/2, \\ 0, & \tau > T/2, \end{cases}$$

$T = 200$ ns, beam current $I_0 = \pi r_0^2 j_0 = 80$ kA, electron energy $\varepsilon = 0.35$ MeV, beam radius $r_0 = 1$ mm.

The one-dimensional simulation yields insight into the qualitative aspects of the processes occurring in the target. Figure 6 shows pressure profiles in the target at various times as a function of $x$. We see that a high pressure region forms initially in the target, and its spatial profile is similar to the energy deposition profile of the REB (the heating takes place at nearly constant volume). A compression wave with an initially continuous profile travels into the target; it becomes steeper with time, and a shock wavefront forms in the flow. Compression waves traveling toward the surface of the target facing the beam are reflected by the target and become decompression waves, which overtake the shock
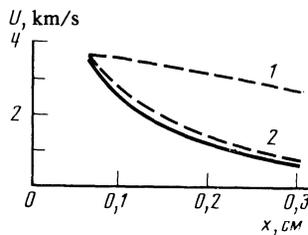


FIG. 7. Damping of the mass velocity $U$ of a shock wave traveling into the target: the solid curve shows experimental results; curves 1 and 2 give values calculated by one- and two- dimensional computer simulation, respectively.

wave and attenuate it. The vaporized metal moves into the beam at high velocity ($\approx 3 \cdot 10^6$ cm/s) and forms a corona with a maximum temperature of 40–50 eV. The shock wave intensity is determined by two competing factors—the energy deposited by the beam, which is responsible for the increased pressure at the wavefront, and decompression waves which arrive from the back side of the target and reduce the pressure.

The dashed line 1 in Fig. 7 shows the calculated mass velocity behind the shock wave as a function of the distance $x$ (one-dimensional case), while the solid curve plots the experimental data. For large $x$, the latter clearly lie well below the calculated values. This is hardly surprising, since the lateral expansion of the target material is considerable here and the shock waves are damped more quickly.

We allowed for the increased damping by carrying out a series of two-dimensional calculations for an axisymmetric flow. Figure 8 shows isobars (in Mbar) inside an aluminum target at times 100, 200, and 300 ns. Figure 8c was calculated at a time after the shock wave was reflected by the back surface and a decompression wave traveled into the target; therefore only the side shock is visible. The dashed curve 2 in Fig. 7 shows the results of the two-dimensional calculations; here the agreement with experiment is quite good (to within 10%). This indicates that the computational model correctly describes the beam-target interaction and, in particular, that the depth of the region in which the REB energy is absorbed is insensitive to collective effects for our target thickness and electron beam parameters.

We observe in closing that the error in the kinematic measurements must be decreased to $\approx 3\%$ if the equation of state is to be used quantitatively in REB experiments at pressures above 1–10 Mbar. This can be done by fabricating the target more carefully and replacing the photomultiplier by an image converter tube. The effects of the transverse decompression waves can be eliminated by making the step as shallow as possible, so that the measurements are carried out as close as possible to the plasma spot, but still far enough away so that there is no appreciable preheating of the target by the electron beam and the measurements are made in the region where the shock wave has already formed. This procedure makes it necessary to use targets $\approx 1$–1.5 mm thick, for which the lateral decompression may be appreciable. The effects of this can be minimized by defocusing the beam (thereby decreasing the amplitude of the shock wave) or by decreasing the size of the energy deposition region by insert-
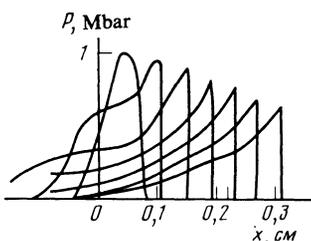


FIG. 6. Pressure profiles in an aluminum target at various times, calculated by one-dimensional computer simulation.

492     Sov. Phys. JETP **62** (3), September 1985
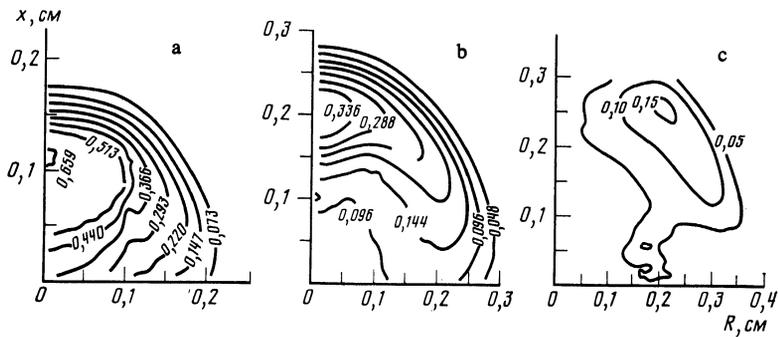
Akkerman *et al.*     492

FIG. 8. Isobars (Mbar) in a 3-mm-thick aluminum target at $t = 100$ ns (a), 200 ns (b), 300 ns (c).

ing a layer of heavy material to strongly absorb the REB behind the target. The choice of the step height itself depends on how effectively the decompression waves reflected by the back side of the target damp the shock wave; gasdynamic calculations give values $\approx 100$–$200\ \mu m$.

[1]A. M. Prokhorov, S. I. Anisomov, and P. P. Pashinin, Usp. Fiz. Nauk **119**, 401 (1976) [Sov. Phys. Usp. **19**, 547 (1976)].

[2]L. J. Rudakov and A. A. Samarsky, in: Sixth Eur. Conf. Controlled Fusion and Plasma Physics, Vol. 1, Moscow (1973), p. 487.

[3]A. V. Bushman and V. E. Fortov, Usp. Fiz. Nauk **140**, 177 (1983) [Sov. Phys. Usp. **26**, 465 (1983)].

[4]Ya. B. Zel'dovich and Yu. P. Raizer, *Physics of Shock Waves and High Temperature Hydrodynamic Phenomena*, 2 vols., Academic Press, New York (1966, 1967).

[5]A. V. Al'tshuler, Usp. Fiz. Nauk **85**, 197 (1965) [Sov. Phys. Usp. **8**, 52 (1965)].

[6]V. E. Fortov, Usp. Fiz. Nauk **138**, 361 (1982) [Sov. Phys. Usp. **25**, 781 (1982)].

[7]F. C. Perry and M. M. Widner, J. Appl. Phys. **47**, 127 (1976).

[8]B. A. Demidov, M. V. Ivkin, V. A. Petrov, *et al.*, Zh. Tekh. Fiz. **50**, 2205 (1980) [Sov. Phys. Tech. Phys. **50**, 1285 (1980)].

[9]Yu. M. Gorbulin, D. M. Zlotnikov, Yu. G. Kalinin, *et al.*, Pis'ma Zh. Eksp. Teor. Fiz. **35**, 332 (1982) [Sov. Phys. JETP **35**, 408 (1982)].

[10]B. A. Demidov, in: Proc. Fourth All-Union Symp. on High-Current Electronics, Vol. 2, Tomsk (1982), p. 264.

[11]V. E. Bespalov, M. M. Bubnov, V. I. Vovchenko, *et al.*, Pis'ma Zh. Tekh. Fiz. **10**, 55 (1984) [Sov. Tech. Phys. Lett. **10**, 24 (1984)].

[12]B. A. Demidov, M. V. Ivkin, and V. A. Petrov, in: Proc. Sixth All-Union Conf. on Charged Particle Accelerators, Vol. 2, Dubna (1979), p. 67.

[13]V. E. Bespalov, L. G. D'yachkov, G. A. Kobzev, and V. E. Fortov, Teplofiz. Vys. Temp. **17**, 266 (1976).

[14]R. J. Trainor, J. W. Shaner, U. M. Auerbach, and N. C. Holmes, Phys. Rev. Lett. **42**, 1154 (1979).

[15]A. V. Bushman, I. K. Krasyuk, P. P. Pashinin, *et al.*, Pis'ma Zh. Eksp. Teor. Fiz. **39**, 341 (1984) [JETP Lett. **39**, 411 (1984)].

[16]A. A. Leont'ev and V. E. Fortov, Zh. Prikl. Mat. Teor. Fiz., No. 3, 162 (1974).

[17]G. S. Romanov and M. V. Suzdenkov, Dokl. Akad. Nauk BSSR **26**, 496 (1982).

[18]A. M. Prokhorov and V. E. Fortov, Usp. Fiz. Nauk **142**, 395 (1984) [Sov. Phys. Usp. **27**, 181 (1984)].

[19]S. L. Bogolyubskii, B. P. Gerasimov, V. I. Liksonov, *et al.*, Pis'ma Zh. Eksp. Teor. Fiz. **24**, 202 (1976) [JETP Lett. **24**, 178 (1976)].

[20]I. P. Afonin, M. V. Babykin, K. A. Bajgarin, *et al.*, in: Seventh Symp. on Engineering Problems of Fusion Research, Knoxville, Tennessee, Oct. 25–28 (1977), p. 269.

[21]A. V. Bushman, A. L. Ni, and V. E. Fortov, in: Uravneniya Sostoyaniya v Éksperimental'nykh Usloviyakh (Equations of State in the Laboratory), ITPM SO AN USSR, Novosibirsk (1981), p. 3.

[22]S. K. Godunov, A. V. Zabrodin, M. Ya. Ivanov, *et al.*, Chislennoe Reshenie Mnoogomernykh Zadach Gazovoĭ Dinamiki (Numerical Solution of Multidimensional Problems in Gas Dynamics), Nauka, Moscow (1976).

[23]A. F. Akkerman, Yu. M. Nikitushev, and V. A. Botvin, Reshenie Metodom Monte-Karlo Zadach Perenosa Bystrykh Élekronov v Veshchestve (Monte-Carlo Calculations of Fast Electron Transport in Matter), Nauka, Alma-Ata (1972).

Translated by A. Mason